Physica A 415 (2014) 294–306

Contents lists available at ScienceDirect

Physica A

journal homepage: www.elsevier.com/locate/physa

Quantum energy and coherence exchange with discrete baths

M. Galiceanu [a], M.W. Beims [b,c,*], W.T. Strunz [d]

[a] Departamento de Fisica, Universidade Federal do Amazonas, 69077-000 Manaus, Brazil
[b] Departamento de Física, Universidade Federal do Paraná, 81531-990 Curitiba, Brazil
[c] Max Planck Institute for the Physics of Complex Systems, Nöthnitzer Strasse 38, 01187 Dresden, Germany
[d] Institut für Theoretische Physik, Technische Universität Dresden, 01062 Dresden, Germany

HIGHLIGHTS

- Quantum coherence of systems coupled to finite baths composed of N harmonic oscillators is investigated.
- A stochastic Schrödinger equation is solved numerically.
- The energy and purity exchange between system and bath are described in details as a function of the numbers of bath harmonic oscillators.
- The non-Markovian dynamics due to finite baths is analyzed.

ARTICLE INFO

Article history:
Received 8 August 2014
Available online 13 August 2014

Keywords:
Discrete baths
Quantum information
Decoherence

ABSTRACT

Coherence and quantum average energy exchange are studied for a system particle as a function of the number N of constituents of a discrete bath model. The time evolution of the energy and coherence, determined via the system purity (proportional to the linear entropy of the quantum statistical ensemble), are obtained solving numerically the Schrödinger equation. A new simplified stochastic Schrödinger equation is derived which takes into account the discreteness of the bath. The environment (bath) is composed of a *finite* number N of uncoupled harmonic oscillators (HOs), characterizing a structured bath, for which a non-Markovian behavior is expected. Two distinct physical situations are assumed for the system particle: the HO and the Morse potential. In the limit $N \to \infty$ the bath is assumed to have an ohmic, sub-ohmic or super-ohmic spectral density. In the case of the HO, for very low values of N ($\lesssim$10) the mean energy and purity oscillate between HO and bath indefinitely in time, while for intermediate and larger values ($N \sim 10 \to 500$) they start to decay with two distinct time regimes: exponential for relatively short times and power-law for larger times. In the case of the Morse potential we only observe an exponential decay for large values of N while for small N's, due to the anharmonicity of the potential, no recurrences of the mean energy and coherences are observed. Wave packet dynamics is used to determine the evolution of the particle inside the system potentials. For both systems the time behavior of a non-Markovianity measure is analyzed as a function of N and is shown to be directly related to the time behavior of the purity.

* Corresponding author at: Departamento de Física, Universidade Federal do Paraná, 81531-990 Curitiba, Brazil. Tel.: +55 33613349.
E-mail address: mbeims@fisica.ufpr.br (M.W. Beims).

http://dx.doi.org/10.1016/j.physa.2014.08.009
0378-4371/

1. Introduction

The quantum dynamics of the physically relevant part in a complex system can be described as the dynamics of few degrees of freedom (the main system) coupled to many degrees of freedom which effectively act as a bath or environment, which may induce dissipation and decoherence [1]. In such a description the bath itself can be highly structured, containing specific modes which strongly influences back the system dynamics. Structured baths have become of significance since they describe realistic situations of non-equilibrium physics. Three major recent examples are the single localized spin 1/2 coupled to a finite spin-polarized environment [2], superconducting quantum bit coupled to an environment composed of a single electromagnetic mode of the cavity [3], and the energy transfer between a light-harvesting protein and a reaction center protein [4]. Understanding the physics encountered in this process will help exploring its huge potential [5]. Thus, theoretical descriptions of general features involving decoherence and quantum energy exchanges of the main system coupled to structured baths are of relevance for non-equilibrium physics processes. The present work is an attempt of such description.

The quantum dissipation and decoherence are analyzed for an open system interacting with its environment by collision processes. The problem (System + Environment + Interaction) is conservative but, due to energy exchange between system and environment, the *system* can be seen as an open system with dissipation. Such a theoretical model has been proposed and studied in quantum [6–8] and classical [7–9] systems. Various models were developed to treat such open systems. We start by mentioning the methods which have focused on an explicit quantum dynamical treatment of the system + bath dynamics: path integral approaches [10–12], the multiconfiguration time-dependent Hartree (MCTDH) technique for wave packet propagation [13], the Gaussian-MCTDH approach [1], the effective-mode representation[14], and the local coherent-state approximation to system–bath dynamics [15]. Another way of studying the system + bath dynamics is to solve the non-Markovian master equations [16–18], including some semiclassical approaches [19,20].

Here a non-Markovian quantum trajectory theory is used, named non-Markovian quantum-state diffusion, that describes the dynamics of a quantum system coupled linearly via position to an environment [21–24]. Differently from most of the previous studies, the environment here is composed by a *finite* number N of uncoupled HOs, as studied recently for classical continuous systems [25,26] and maps [27]. In such cases we say to have a discrete or structured bath. As discussed later, such a discrete bath may induce a non-Markovian evolution in the system. Some experiments in which the non-Markovian behavior arises due to the discreteness of the bath can be mentioned: high-Q microwave cavities, quantum optics in materials with a photonic band gap, output coupling from a Bose–Einstein condensate to create an atom laser [28–32] or the decoherence phenomenon [33–36]. From the classical point of view, in the context of finite baths with uncoupled HO, there are some works which analyze the effect of discrete (structured) baths on the system energy decay [9,25,26] and on ratchet transport [37,38]. The main result found is that finite baths may induce a non-Markovian dynamics on the system particle. From the quantum point of view, most works [1,9,15,20,36,39] focus on the analysis of changing the frequency distributions and the coupling strength between system and bath. In a distinct context analytical results [40] studied the time evolution of the concurrence and the purity of two interacting qubits embedded in finite and infinite numbers of environmental spins. However, no recurrences are analyzed. Application to finite quantum thermostats was also discussed [41].

We analyze systematically the effect of increasing the number of oscillators N from the bath on the system energy and purity decay. In most cases we vary $N = 1 \to 500$. As N increases, the quantum simulations need long computational times since they were realized over many realizations of the bath. Usually we use 1000 realizations but, when specified, we needed more. For very low values of N the mean time energy and the purity decrease but comes back to the same initial value. This energy exchange (and the purity behavior) between system and bath continues for larger times. For intermediate and larger values of N ($10 \lesssim N \lesssim 500$) the initial energy inside the system and the purity never return back to the system (for the integrated times) and suffer a transition from exponential decays for shorter times to power-law decays for larger times.

The paper is organized as follows. In Section 2 we introduce the basic concepts of non-Markovian quantum-state diffusion and derive a new simplified stochastic Schrödinger equation valid for *finite* baths. In Section 3 the simplified equation is applied to analyze the N dependence of some useful physical quantities such as the energy decay, the average position, and the purity (decoherence). In this section the harmonic potential is considered. In Section 4 a Morse potential is used for the system particle. In the last section we present a summary and the conclusions.

2. Linear non-Markovian quantum-state diffusion

The non-Markovian quantum-state diffusion (QSD) equation is based on a standard model of open system dynamics: a quantum system interacting with a bosonic environment with the total Hamiltonian

$$H_{tot} = H + \sum_{\lambda} g_{\lambda}(La_{\lambda}^{+} + L^{+}a_{\lambda}) + \hbar \sum_{\lambda} \omega_{\lambda} a_{\lambda}^{+} a_{\lambda}, \tag{1}$$

where H is the Hamiltonian of the system of interest, L is a system operator coupling to environment and a_{λ}^{+}, a_{λ} are the raising and lowering operators, with the property $[a_{\lambda}, a_{\lambda'}^{+}] = \delta_{\lambda\lambda'}$. The linear non-Markovian QSD equation [23,24,42–44] is given by

$$\hbar \left| \frac{\partial}{\partial t} \psi_t \right\rangle = -\mathrm{i}H' \left|\psi_t\right\rangle + Lz_t^{*} \left|\psi_t\right\rangle - L^{+} \int_0^t \mathrm{d}s K(t-s) \frac{\delta \left|\psi_t\right\rangle}{\delta z_s^{*}}, \tag{2}$$

where was assumed a factorized total initial state $|\psi_0\rangle = |0_1\rangle\,|0_2\rangle\cdots|0_\lambda\rangle\cdots$, with an arbitrary system state $|\psi_0\rangle$ and all environmental oscillators in their ground state $|0_\lambda\rangle$. H' is a (possibly environment-renormalized) system Hamiltonian, the time-dependent C-number

$$z_t^* = -\mathrm{i}\sum_\lambda g_\lambda^* z_\lambda^* \mathrm{e}^{\mathrm{i}\omega_\lambda t} \tag{3}$$

is a complex Gaussian process with zero mean and correlations $M[z_t^* z_s] = K(t-s) = \sum_\lambda |g_\lambda|^2 \mathrm{e}^{-\mathrm{i}\omega_\lambda(t-s)}$, where $M[]$ denotes the *ensemble average* over this classical driving noise. The form of $K(t-s)$ corresponds to the zero-temperature limit. The index λ enumerates the oscillator of the bath, g_λ is the coupling to oscillator λ, ω_λ is its frequency and $z_\lambda^* = (x_\lambda + iy_\lambda)/\sqrt{2}$, where (x_λ, y_λ) are normal (Gaussian) distributed real numbers with zero mean and deviation one. The many realizations to solve the stochastic Schrödinger equation are done over these normally distributed numbers. Using perturbation theory in the system selfcoupling strength, the functional derivative of Eq. (2) can be written in the first order approximation as a linear function of $|\psi_t\rangle$ [45]

$$\frac{\delta\,|\psi_t\rangle}{\delta z_s^*} = O(t,s,z^*)\,|\psi_t\rangle \approx \mathrm{e}^{-\mathrm{i}H(t-s)} L \mathrm{e}^{\mathrm{i}H(t-s)}\,|\psi_t\rangle\,. \tag{4}$$

During the simulations in Sections 3 and 4, we use the first order approximation with the system operator, $L = L^+ = q$, which is the position operator of the system. Using the last equation, the stochastic Schrödinger equation becomes

$$\hbar\frac{\partial}{\partial t}\,|\psi_t\rangle = -\mathrm{i}H'\,|\psi_t\rangle + q z_t^*\,|\psi_t\rangle - q\int_0^t \mathrm{d}s K(t-s)\mathrm{e}^{-\mathrm{i}H'(t-s)} q \mathrm{e}^{\mathrm{i}H'(t-s)}\,|\psi_t\rangle\,. \tag{5}$$

In Eqs. (2) and (5), the Hamiltonian $H' = H(q,p) + q^2 A(t)$, with $A(t) = \sum_\lambda \frac{|g_\lambda|^2}{\omega_\lambda}(\cos\omega_\lambda t - 1)$, contains an additional potential term that turns out to be counterbalanced by a similar term arising from the memory integral [43]. Using $|\psi_t\rangle = \sum_n c_n(t)\,|\phi_n\rangle$, $H\,|\phi_n\rangle = \epsilon_n\,|\phi_n\rangle$, $q = \sum_{n,m} q_{nm}\,|\phi_n\rangle\,\langle\phi_m|$, and orthonormal condition $\langle\phi_n|\phi_{n'}\rangle = \delta_{nn'}$, Eq. (5) transforms to

$$\hbar\dot{c}_n(t) = -\mathrm{i}\epsilon_n c_n(t) - \mathrm{i}A(t)\sum_{mm'} q_{nm}q_{mm'}c_{m'}(t) + z_t^*\sum_m q_{nm}c_m(t) - \sum_{m,m'} q_{nm'}\bar{O}_{mm'}(t)c_{m'}(t), \tag{6}$$

where

$$\bar{O}_{mm'}(t) = \left\langle\phi_m|\bar{O}(t)|\phi_{m'}\right\rangle = q_{mm'}\sum_\lambda |g_\lambda|^2 \frac{\mathrm{e}^{-\mathrm{i}[\omega_\lambda + (\epsilon_m - \epsilon_{m'})]t} - 1}{-\mathrm{i}[\omega_\lambda + (\epsilon_m - \epsilon_{m'})]}, \tag{7}$$

and

$$\bar{O}(t) = \int_0^t \mathrm{d}s K(t-s)\mathrm{e}^{-\mathrm{i}H(t-s)} q \mathrm{e}^{\mathrm{i}H(t-s)}. \tag{8}$$

We call to attention that the operator $\bar{O}(t)$ is the memory integral. When N is finite we always expect some memory effects and, in this sense, a non-Markovian behavior.

For simplicity, we choose the Planck constant $\hbar = 1$ throughout the paper. The *quantum expectation* of the energy is given by

$$\langle E\rangle = \langle\psi_t|H|\psi_t\rangle = \sum_n c_n^*(t)c_n(t)\epsilon_n, \tag{9}$$

while the *quantum expectation* for the position is

$$\langle q\rangle = \langle\psi_t|q|\psi_t\rangle = \sum_{n,m} c_n^*(t)c_m(t)q_{nm}. \tag{10}$$

Now the stochastic Schrödinger equation coupled to a finite bath, Eq. (6), will be implemented to calculate the energy decay for the system particle inside two types of potentials, widely used in physics: the harmonic potential and the Morse potential. We also consider the time evolution of the quantum average position.

For later purposes we write an approximate expression for the damping coefficient due to finite baths. For this we assume that the system dynamics is approximately harmonic. For very small couplings, the system HO can be roughly assumed to be independent of the bath. Thus the HO solution for $\mathrm{e}^{-\mathrm{i}H(t-s)} q \mathrm{e}^{\mathrm{i}H(t-s)}$ can be obtained analytically and inserted in Eq. (8). Knowing [6,9] that $K(t-s) = \sum \frac{g_\lambda^2}{\omega_\lambda}\cos\omega_\lambda(t-s)$ the integration of (8) leads to $\bar{O}(t) \sim \gamma(t)\dot{q}(t)$, where

$$\gamma(t) = \sum_\lambda^N \frac{g_\lambda^2}{2\omega_\lambda^2}\left[\frac{\sin(\Delta\omega_+)t}{\Delta\omega_+} + \frac{\sin(\Delta\omega_-t)}{\Delta\omega_-}\right], \tag{11}$$

is the time dependent damping coefficient, where $\Delta\omega_- = \omega_\lambda - \omega$ and $\Delta\omega_+ = \omega_\lambda + \omega$. It is dependent on time, system frequency ω, bath frequencies ω_λ, coupling strength g_λ and N. The function $\gamma(t)$ has a slower oscillation with times

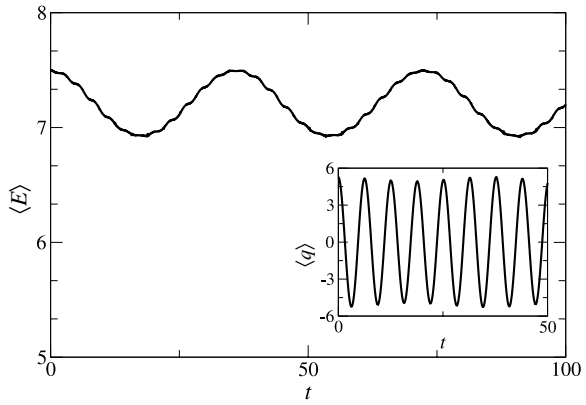

Fig. 1. The average energy of a system, Eq. (9), coupled to a bath of one HO, with the coupling strength $g = 0.008$. Inset shows the corresponding average position, Eq. (10).

$t_{slow} = 2\pi/\Delta\omega_-$ and large amplitude $(1/\Delta\omega_-)$, when compared to the fast oscillations at times $t_{fast} = 2\pi/\Delta\omega_+$ and smaller amplitude $(1/\Delta\omega_+)$. The above formula will be used later and it is of relevance since it is related to the average energy (9) by the following relation

$$\Gamma(t) = \mathrm{e}^{-\int_0^t \gamma(t')\mathrm{d}t'} \propto \langle E(t)\rangle. \tag{12}$$

The expression (12) should be approximately valid for the HO results shown in Section 3 and for very small energies for the Morse potential results from Section 4.

3. Harmonic potential coupled to *N* oscillators

In this section we consider a particle inside a harmonic potential coupled to a discrete bath of N HOs with frequencies ω_λ distributed in the interval (0.1, 1.0). These frequencies are picked randomly from a frequency generator, but once picked they will be kept fixed during the simulations, even for different bath realizations. In this approach, due to the finite number of HOs in the bath, the spectral density is determined numerically and is always structured for low values of N (see Ref. [25] for more details in the classical case). The properties of the bath depend on the frequency's distribution of the N HOs [25]. The frequency generator is chosen so that in the limit $N \to \infty$ we have three distinct continuous distributions: ohmic bath (quadratic), sub-ohmic and super-ohmic. Each oscillator will have a distinct (x_λ, y_λ) pair, randomly chosen numbers with zero mean and deviation one. For each coefficient c_n of Eq. (6) we consider rectangular initial conditions: $c_n(0) = 1/\sqrt{n_{max}} + 0 \cdot i$, with $n = 1, \ldots, n_{max}$, where n_{max} is the last energy level considered. The first $n_{max} = 15$ energy levels from the harmonic potential are considered, with energy $E_n = \hbar\omega(n - \frac{1}{2})$. Using $\omega = \hbar = 1.0$ the ground state energy level equals 0.5. Thus our initial state is given by

$$|\psi_0\rangle = \frac{1}{\sqrt{n_{max}}} \sum_{n=1}^{n_{max}=15} |\phi_n\rangle\,, \tag{13}$$

which is a coherent superposition of all 15 system levels. In order to obtain the energy decay as a function of time and the average position as a function of the number of oscillators in the bath, Eq. (6) is integrated by a fourth-order Runge–Kutta integrator [46] and the values of $c_n(t)$ are introduced in Eqs. (9) and (10). In the first part of this section the frequencies of the harmonic oscillators from the bath will follow a quadratic distribution, making the spectral density a linear function $J(\omega \le \omega_{cut}) \propto \omega$ when $N \to \infty$. To render the comparison easier the coupling strength of each oscillator from the bath equals $g_\lambda = 0.008/\sqrt{N}$. This effective coupling is needed so that the effect of the environment over the HO converges as N becomes large [47].

3.1. The system energy

In Fig. 1 the time evolution of the average energy $\langle E\rangle$, Eq. (9), is plotted for a bath containing one HO with the frequency $\omega = 0.82$. In the inset of Fig. 1 the average position $\langle q\rangle$ from Eq. (10) is displayed. One can clearly see that, besides the tiny (amplitude) fast oscillations at times $t_{fast} = 2\pi/\Delta\omega_+ \sim 3.50$, for times $t_d = t_{slow}/2 = \pi/\Delta\omega_- \sim 17.5$ the system loses around 15% of its initial energy to the bath, but is able to regain it at a later time $t_R = t_{slow} \sim 34.9$. This exchange of energy between system and environment will repeat itself, with frequency around $\Delta\omega_- \sim 0.18$, for all integrated times (we checked it until $t = 1000$). Thus, the mean energy over the return times, or recurrences times (where the energy transferred into the bath returns to the system) is almost constant. The return times of the energy are dependent on the frequency of the bath oscillator.

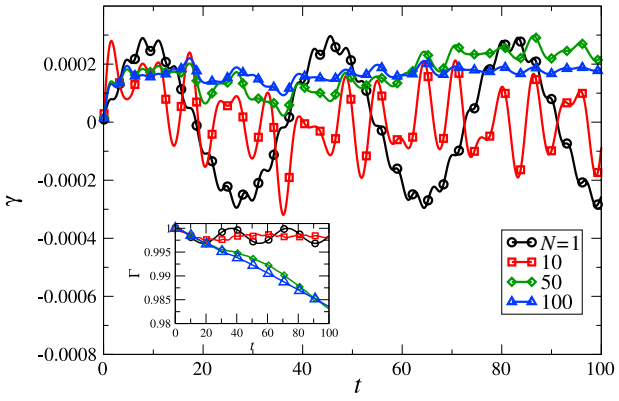

Fig. 2. Time dependent dissipation $\gamma(t)$ from Eq. (11) for $N = 1, 10, 50, 100$. In the inset is plotted Eq. (12).

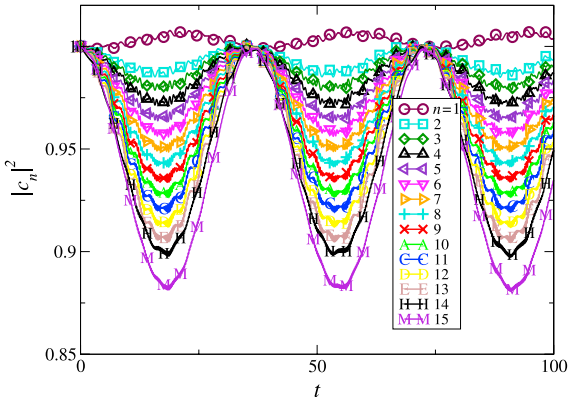

Fig. 3. The time evolution of all 15 states probabilities $|c_n|^2$ of a system coupled to a bath of one HO.

To understand better the observed energy exchange and the dissipation process in such finite baths, we use the expression for the approximate damping $\gamma(t)$ from Eq. (11). It is plotted in Fig. 2 for different values of N. For $N = 1$ we see that $\gamma(t)$ is negative for times $t_{slow}/2 = 17.5 \lesssim t \lesssim t_{slow} = 34.9$. Thus, for these times the energy should be injected from the bath to the system. Indeed, these are the times where the energy returns to the system in Fig. 1. In the inset graph of Fig. 2 we plot $\Gamma(t)$, which is proportional to the average energy, Eq. (12). Comparing Figs. 1 and 2 (for $N = 1$) one can clearly observe the similarity.

The time dependence of the energy was also confirmed by the time evolution of the average position: the system symmetrically oscillates very fast around the center $\langle q \rangle = 0$, with an amplitude which follows the pattern of energy decay. Namely, the minimum of the energy corresponds to the minimum of the highest system oscillator amplitude.

Fig. 3 shows the time evolution of all the 15 individuals energy levels of the harmonic potential for the same bath used in Fig. 1. Numbers denote the energy quantum number n, namely the curve denoted by $n = 1$ shows the time evolution of the ground state probability, $|c_1|^2$, with $n = 2$ denotes the values of the probability for the second energy level, $|c_2|^2$, and so on. One can clearly notice that while the lowest states remain practically unchanged, the higher energy levels oscillate following the energy exchange observed in Fig. 1. Thus only the higher states are responsible for the energy exchange.

In Fig. 4 the energy decay is shown in a linear plot for a bath of $N = 10$ HOs. In the time limit studied here ($t_{max} = 100$) one can clearly see that the system energy will not be regained, so that the time average from the system energy is not constant anymore. However, we expect that for some later times $t > t_{max}$ the energy will return to the system, since it is a finite system. The qualitative behavior of the energy decay rate changes for different time intervals. We show by symbols the best fits of the energy decay, namely an exponential fit, $\alpha = 0.0027$, for short times, followed by another exponential fit with $\alpha' = 0.0038$ and one power-law fit, $\beta = 0.0093$, for later times. We say that the qualitative change from exponential to power-law decay occurs close to times $t_{\alpha\to\beta}$. As an inset graph we display the corresponding average position. The time evolution of all the 15 states probabilities $|c_n|^2$ of the system coupled to a bath which has $N = 10$ HOs, is displayed in Fig. 5. As in Fig. 3, $n = 1$ shows the probability of the lowest energy level, $|c_1|^2$, $n = 2$ corresponds to the second energy level and so on. Again it is clear that the higher energy levels decay faster. Something similar was shown to occur with the decoherence rate which is correlated to the highest occupied states [48].

The energy decay and the average position for a bath of $N = 100$ harmonic oscillators is displayed in Fig. 6. The system continues to behave dissipatively for the integrated time, with an exponential decay, $\langle E \rangle \propto \exp(-0.0049t)$ for $0 < t \lesssim 10$

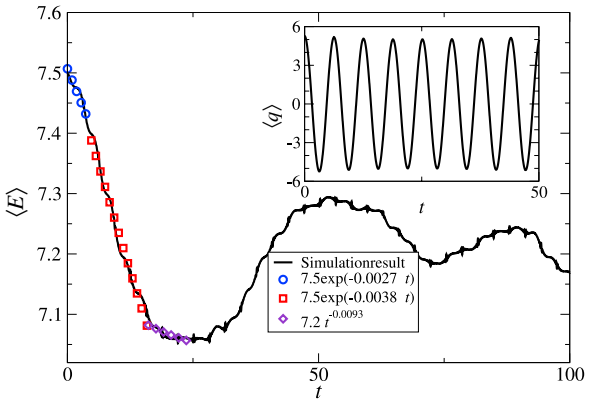

Fig. 4. The average energy decay, Eq. (9), for a bath of 10 HOs, with the total coupling strength equal to 0.008. We display the best fits with symbols. In the inset is shown the average position, Eq. (10).

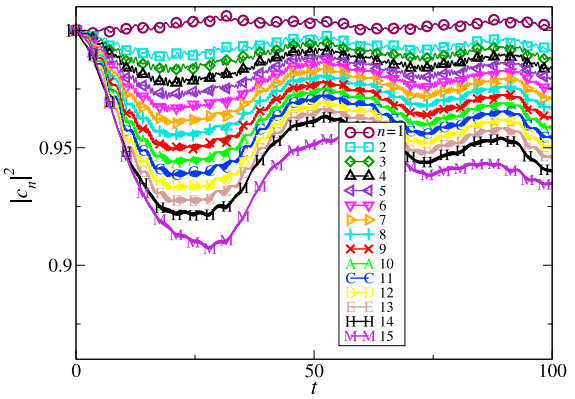

Fig. 5. The time evolution of all 15 states probabilities $|c_n|^2$ of a system coupled to a bath containing $N = 10$ HOs.

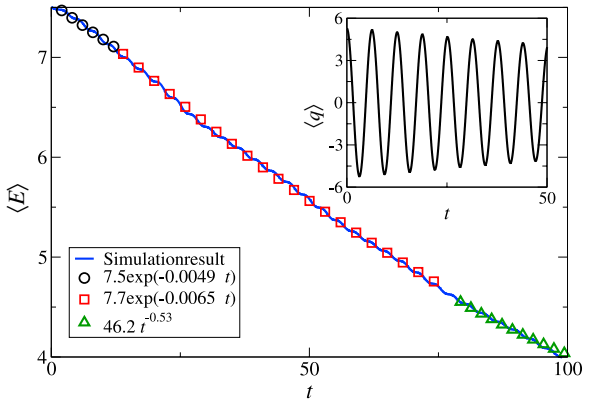

Fig. 6. The average energy and its best fits for a bath of $N = 100$ harmonic oscillators. As an inset we show the average position.

and a power-law decay $\langle E\rangle \propto t^{-0.53}$ for much larger times $t \gtrsim 80$. For an intermediate time region, starting at $t \sim 10$ and ending at $t \sim 75$, an additional exponential decay, $\langle E\rangle \propto \exp(-0.0065t)$, was observed. Such kind of behaviors with two exponential decays and a power-law decay was also encountered for $N \geq 100$.

In Fig. 7 we summarize results of the energy decay for $N = 1, 10, 20, 50, 100, 500$ HOs. The first observation is that the energy decays faster for larger N. For values $10 \geq N \geq 50$ we observe an exponential decay for shorter times, another exponential decay for intermediate time domain and a power-law decay for larger times, immediately followed by an increase in energy. These values of N correspond to a transient regime from an almost conservative situation ($N < 10$), where the mean energy over oscillations is almost constant, to a dissipative-like one ($N \geq 100$), where, for the integrated times the energy only decays. Details of the decay exponents will be discussed later in Figs. 11 and 12. As N increases the

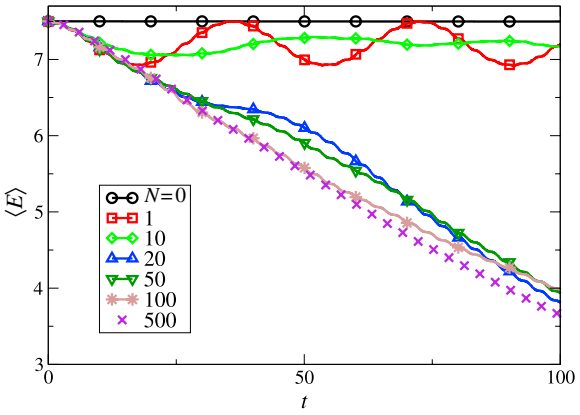

Fig. 7. The energy decay for a bath with $N = 1, 10, 20, 50, 100, 500$ HOs. For $N \geq 10$ we observe exponential decays followed by power-law decay.

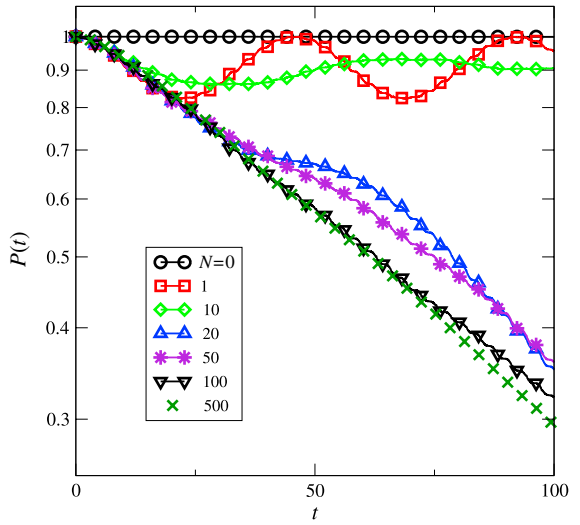

Fig. 8. The purity for a bath with $N = 1, 10, 20, 50, 100, 500$ HOs.

second exponential decay gets more evident and power-law decay becomes more pronounced and larger. Remarkably the behavior for small Ns is mapped by the curve of highest N: for instance the parameter α' of the second exponential behavior is almost the same for all $N \geq 10$.

3.2. The system linear entropy and purity

Instead of looking at the dissipation, it is also possible to analyze the linear entropy S_L of the quantum statistical ensemble. It quantifies the degree of ignorance about the system state and can be calculated from $S_L(t) = 1 - P(t)$. Here $P(t) = \mathrm{Tr}_c\left[\rho_s^2(t)\right]$ is the purity which gives information about the decoherence occurred in the system and $\rho_s(t) = \overline{\overline{|\psi_t\rangle\langle\psi_t|}}$ is the reduced density matrix. For our initial coherent state from Eq. (13), the initial reduced density matrix $\rho_s(0)$ has 15 diagonal terms and 15 off-diagonal terms. The off-diagonal terms are characteristic of the quantum coherence. Total decoherence of the initial state occurs at times t_{dec} when all off-diagonal terms vanish. For these times a statistical mixture of the 15 diagonal terms is reached and the purity of the reduced density matrix is $P(t_{dec}) = 1/15 \sim 0.067$. In this way it is possible to compare total decoherence times t_{dec} with dissipation times.

In Fig. 8 we plot the time evolution of the purity for the same parameters shown in Fig. 7. For $N = 0$ (no bath) the purity keeps constant to 1. For $N = 1$ the purity diminishes and increases in time, but no total decoherence is observed. For $10 \leq N \leq 100$ we encounter the transient regime observed for the energy: two exponential and a power-law decays followed by an increase of purity. For short times the curves for smaller Ns follow the master curve given by the highest N (500 in our case). For $N \geq 100$ one notices two exponential decays with decay exponent $\sim$0.007 for times $t \lesssim 10$ and another exponential decay with exponent $\sim$0.011 for times $10 \lesssim t \lesssim 50$. For later time the purity decay obeys a power-law decay, as for the energy decay, with the exponent equal to 1.13. In this case the total decoherence was not observed for the integrated times, easily seen since the values of purity are higher than the crossover value $P = 0.067$.

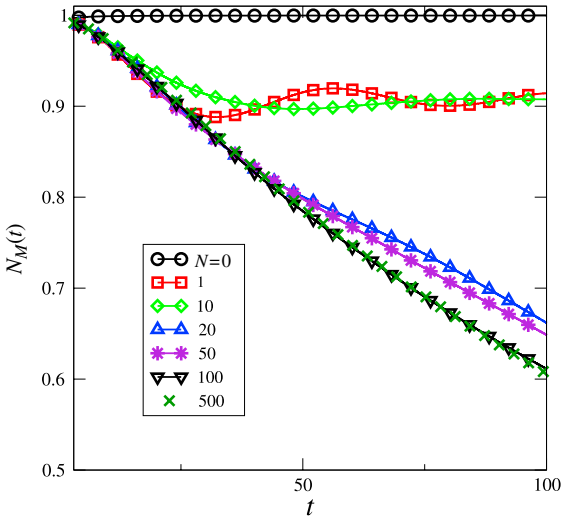

Fig. 9. Non-Markovianity as a function of time for $N = 0, 1, 10, 20, 50, 100, 500$.

All features shown for the energy and coherence decay in time can be roughly explained using the damping coefficient $\gamma(t)$ from Eq. (11) in Eq. (12). For larger values of N Fig. 2 shows that $\gamma(t)$ still oscillates but did not become negative, and the system is expected to behave dissipatively with increasing decoherence. In the inset graph we plot $\Gamma(t)$, and comparing Figs. 2 and 7 we can say that it roughly explains the complicated energy decay and decoherence.

3.3. Measuring the non-Markovianity

As observed in the simulations for the purity, a characteristic coming from finite baths is that the system decoherence oscillates in time. This is directly related to the energy exchange between system and bath. It has been observed [49] that the backflow of quantum correlations can have his origin when non-Markovian finite baths are considered. Thus, it would be interesting to check the relation between oscillations in quantum coherences and the non-Markovian behavior. In the context of the present work it is very appropriate to define the non-Markovianity measure [50–52] as

$$N_M(t) = \frac{1}{t}\int_0^t \mathrm{d}t' \left|P(t')\right|, \tag{14}$$

which increases with the number of recurrences of the purity. It is maximal for $N_M(t) = 1$ and zero in the Markovian limit. In Fig. 9 the quantity $N_M(t)$ is plotted for distinct values of N. For $N = 0$, the case of no bath, $N_M(t)$ remains constant equal to one, as expected. For $N = 1$ and 10, $N_M(t)$ decreases to $\sim$0.9 and starts to show some small oscillations in time. These oscillations can be explained using Eq. (11) for the time behavior of the mean energy. Since the purity follows the time behavior of the energy, for $N = 1$ we can approximately write $P(t) \propto 1 - \cos(\omega_- t)$ (neglecting the fast oscillations ω_+). In this case $N_M(t) \propto 1 - \sin(\omega_- t)/t$ which oscillates and has an amplitude which decreases in time. This is exactly the behavior observed in Fig. 9 for $N = 1$ and approximated for $N = 10$. While for $N = 1$ the energy and purity return totally to its initial value at $t = 0$, the non-Markovianity does not. In other words, when recurrences of the purity start to occur, the non-Markovianity becomes constant on average. As N increases to 50, 100, 500, $N_M(t)$ decreases for all integrated times. For $N \to \infty$, $N_M(t)$ is expected to decay very fast. Concluding, while recurrences observed for small values of N induce a finite constant non-Markovianity measure, the exponential and power-law decays of the purity decide how fast the non-Markovianity disappears.

3.4. The phase–space dynamics

Fig. 10 shows the phase space dynamics for one realization of the bath and for different values of $N = 0, 1, 10, 20, 50, 100, 500$. For $N = 1$ the evolution occurs over a circle with a small width. When N increases, this circle starts to look like a ring with a larger and larger width. At $t = 0$ the particle starts on the outer side of the circle. As times goes on, part of its energy is transferred to the bath moving towards the inner side of the circle. Since there is a continuous energy exchange between system and bath, we expect that the particles moves continuously between the inner and outer sides of the circle. Particle does not loose more energy by increasing the number of oscillators in the bath. This is due to the fact that the total coupling strength is the same in all cases: 0.008.

Summarizing, the general observed behavior for the mean energy and the purity is that, for shorter times $t \lesssim t_{disc} \approx 20$ (obtained from the simulations) the exponential decay is independent of N since the system did not have time to resolve the

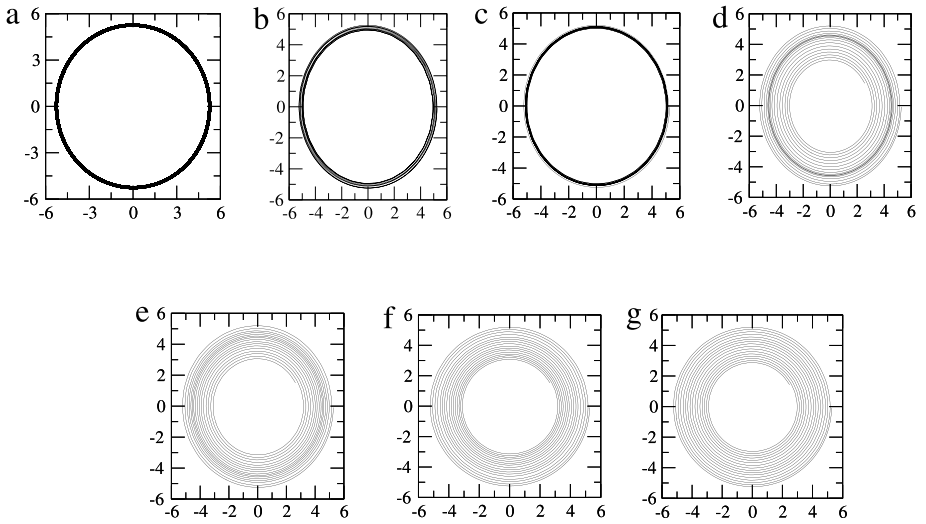

Fig. 10. Phase space dynamics for $N = 0, 1, 10, 20, 50, 100, 500$ (from left to right and top to bottom).

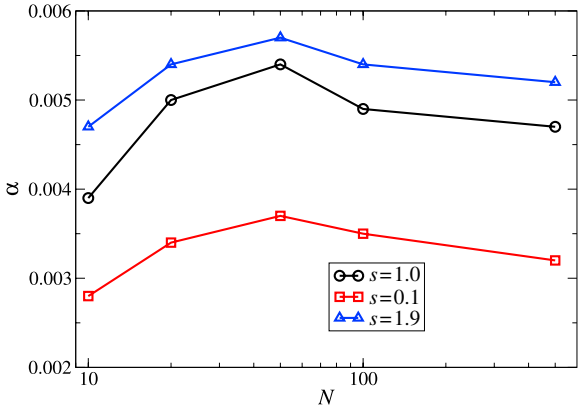

Fig. 11. Exponential fits, α, of the energy decay in the low times region for ohmic, sub-ohmic, and super-ohmic baths as a function of N.

discreteness of the bath. The system behaves as for a continuous bath. After that, for times $t \gtrsim t_{disc}$, the discreteness of the bath is recognized by the system and the N dependence becomes visible. For smaller N, the discreteness makes the mean energy tend to return to the system and the purity tends to increase again. This return still obeys an exponential behavior. Thus, for small values of N the discreteness of the bath only induces the return of the energy to the system. For intermediate values of N, the effect of the energy return to the system is reduced, but a power law behavior appears. For large N the bath spectral density tends to a continuous, but with a power law decay, instead the exponential. The reason is that the discreteness still induces the power law decay.

3.5. Ohmic, sub-ohmic and super-ohmic baths

Now we turn our attention to other types of distributions, we consider the cases for which the spectral density has the form $J(\omega) = \omega^s$, with $0 \leq s \leq 2$ [6]. If $s = 1$ the quadratic frequency distribution of the ohmic bath is recovered. For $s \leq 1$ we have the sub-ohmic bath, where lower frequencies in the chosen domain have a bigger contribution when N is sufficiently large. For $s \geq 1$ we have the super-ohmic case, where higher frequencies appear more frequently.

In Fig. 11 we plot the α exponents of the short time exponential decay for all the three types of baths: ohmic ($s = 1.0$), sub-ohmic ($s = 0.1$), and super-ohmic ($s = 1.9$). One can notice small differences from one type of the bath to another. Immediately apparent is that there are also small differences between Ns, for all the three types of baths. In general, these differences are smaller than 10^{-3} order of magnitude.

In Fig. 12 we plot the β power-law exponents of the long times energy decay for ohmic, sub-ohmic, and super-ohmic baths. Different than the exponents from the exponential behavior, we noticed differences of the order of 0.2 in the exponents of different bath's type. We notice a significant increase of β when N increases.

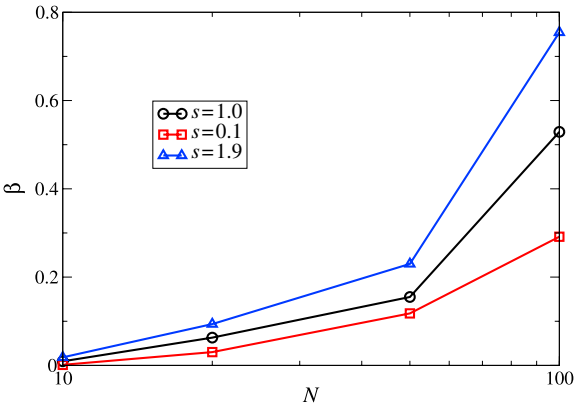

Fig. 12. Power-law fits, β, of the energy decay in the long times region for ohmic, sub-ohmic, and super-ohmic baths as a function of N.

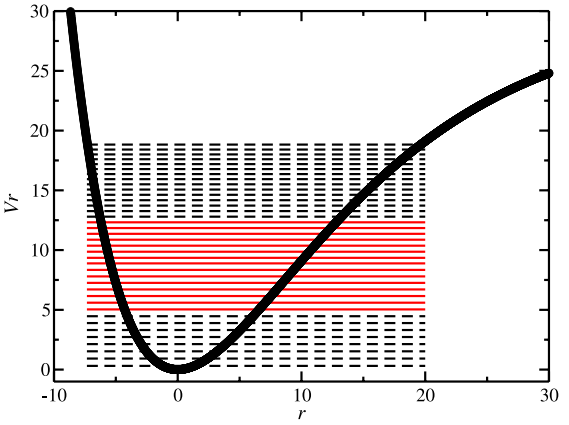

Fig. 13. Morse potential for $D_e = 30$, $a = 0.08$, $r_e = 0$. Horizontal lines depict the energy levels in the r interval $[-7.4, 20]$, while continuous lines show the middle energies levels used in our simulations (see text for details).

4. Morse potential

The Morse potential [53–55] is anharmonic and given by

$$V(r) = D_e[1 - \mathrm{e}^{-a(r-r_e)}]^2, \tag{15}$$

where r is the distance between atoms, r_e is the equilibrium bound distance, D_e is the well depth, $a = \sqrt{\frac{K_e}{2D_e}}$ is the depth. K_e is the force constant at the minimum of the well. The energy levels ϵ_n and the position elements r_{nm} were determined by using the Numerov method [56,57]. The results for the energy levels were compared to the analytical form [53]:

$$\epsilon_n = \left(n + \frac{1}{2}\right)\hbar\omega_M - \frac{\left[(n + \frac{1}{2})\hbar\omega_M\right]^2}{4D_e}, \tag{16}$$

with $\omega_M = a\sqrt{\frac{2D_e}{m}}$ being the mean frequency of the anharmonic oscillation. Fig. 13 shows in thick continuous line the Morse potential, given by Eq. (15), with the following values of the constants [54]: $D_e = 30$, $a = 0.08$, $r_e = 0$ (with $m = 1$ this gives $\omega_M \sim 0.62$). Horizontal lines depict all the 38 energy levels, as calculated from the Numerov method. Due to the anharmonic potential the energy levels are not equidistant as in the HO case.

For the simulations we used as initial condition for the coefficients c_n a Gaussian wave packet form $\phi(r) = C \exp -\frac{(r-16)^2}{\sigma^2}$, where $\sigma = 3$ and C is the normalization constant. Thus, we will have a wave packet with the peak at the energy level 16, placed in the middle of the energy spectrum, corresponding to the values from 5.03 to 12.32, depicted by continuous horizontal lines in Fig. 13. Here, the coefficients c_n have the real Gaussian form defined above and they fulfill the equation $\sum_{n=9}^{23} |c_n|^2(0) = 1$.

The energy decay, Eq. (9), for a bath having $N = 1$, 10, 50, and 100 HOs is plotted in Fig. 14. It was considered that all of them have the same mass $m = 1$ and experience the effective coupling strength with the system, $g_\lambda = g = 0.008/\sqrt{N}$. Thus,

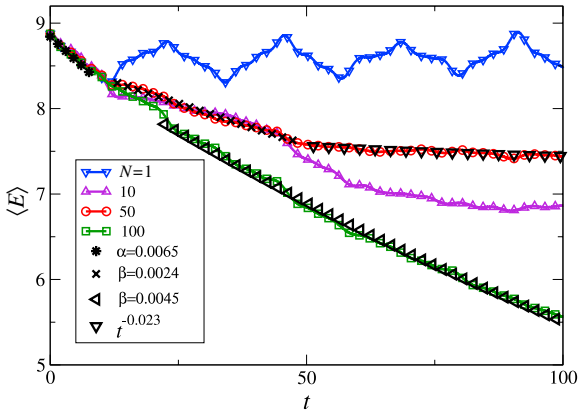

Fig. 14. The energy decay, Eq. (9), for Morse potential. The number of HOs in the ohmic bath is varied: 1, 10, 50, 100.

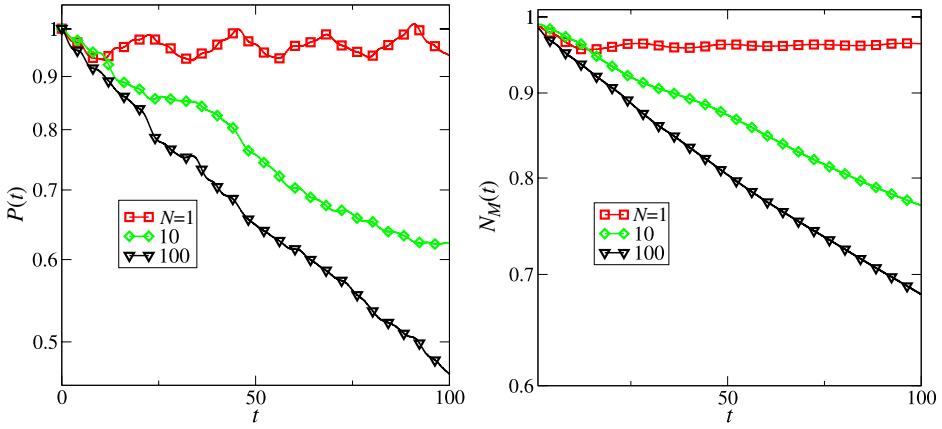

Fig. 15. (a) Purity and (b) non-Markovianity as a function of time for $N = 1, 10, 100$.

again they follow a quadratic distribution in the interval (0.1, 1.0), and for each bath, once chosen the frequencies, they are kept constant. For each case, namely a bath having $N = 1, 10, 50$, and 100 HOs, we will vary only x_λ and y_λ, which are real distributed numbers with zero mean and deviation one. Due to the high CPU time we average over different number of initial conditions and maximum time length, t_{max}. For the simulations we consider all the energy levels of the system, described by a wave packet of 38 energy levels, ϵ_n, corresponding to 38 wavefunctions, ϕ_n (and implicitly the c_n coefficients). As mentioned before, the initial conditions of the coefficients c_n are considered to be 0, except for the 15 intermediate levels, namely from energy level 9 to level 23, which are Gaussian distributed.

In Fig. 14 we plot the results for $N = 1, 10, 50$, and 100 with at least 850 initial conditions. When needed the number of initial conditions was increased, for example $N = 50$ and $N = 100$, and for all the cases $t_{max} = 100$. Immediately apparent is that for $N = 1$ the system regains the energy after $t \sim 25$, comparable with $t_{slow} = 2\pi/\Delta\omega_- \approx 30$. In this case the fast tiny oscillations occur around $t = t_{fast} = 2\pi/\Delta\omega_+ \approx 4.3$. One can easily notice that the results for all $N \geq 10$ values are very similar for short times, until $t \sim 10$: we have an exponential decay with the exponent equal to 0.0065. This exponential decay stops at $t \sim 20$. For longer times ($t \gtrsim 30$) we encounter exponential decays, with the exponent being N-dependent, i.e. 0.0024 for $N = 50$ or equal to 0.0045 for $N = 100$. It is worth to mention that for long times ($t \gtrsim 60$) for a bath with $N = 50$ the best fit is a power-law with the exponent equal to 0.023. Fluctuations are due to the stochastic average. The essential distinction here when compared to the HO case is that, for small values of N ($N = 10$ and 20), we did not observe the return of the energy to the system. The explanation for this must be the anharmonic property of the Morse potential.

For completeness, we also show the behavior of the purity and the non-Markovianity for the Morse case. They are plotted respectively in Fig. 15 (a) and (b) for $N = 1, 10, 100$. As for the HO case, the behavior of the purity basically follows the energy decay and recurrences. For $N = 1$ it oscillates and recurrences are evident. For $N = 10, 100$ it decays for all the integrated times. For the non-Markovianity we observe in Fig. 15(b) that for $N = 1$ it initially decays and after times around 20 it keeps constant, and no recurrences are observed. For $N = 10, 100$ only the exponential decays of the non-Markovianity are observed.

5. Conclusions

In this paper we use the stochastic Schrödinger equation for zero temperature to study the energy and coherence decay for a system particle, under the influence of a harmonic potential and a Morse potential. The system is coupled to a bath composed of a finite number N of uncoupled harmonic oscillators. For the discussions we chose, in the limit $N \to \infty$, an ohmic bath distribution, but we also study the cases of sub-ohmic and super-ohmic baths. In the case of a harmonic potential, with effective coupling intensity to the bath $g = 0.008/\sqrt{N}$, it was observed that for very small numbers N the energy is exchanged back and forth with the bath. For intermediate values of N around $10 \leq N \leq 20$, the time average energy of the system starts to decay, transferring partially its energy to the bath and we do not see any energy regain for the integrated times. For these values of N we observed two exponential energy decays (with different exponents) for small times and a power-law decay for large times. For relatively higher values of N ($\gtrsim$50), the same exponential decays were observed and a more pronounced power-law behavior. We analyzed also the linear entropy of the quantum system state by determining the purity of the system, which gives information about the decoherence process. Essentially, decoherence follows the qualitative behavior of the mean energy. For a system situated in a Morse potential, to render the comparison easier between the harmonic case and the Morse potential we used the same effective coupling strength and the same frequencies of the bath. In this case we have an exponential decay for short times and another exponential decay for longer times. Similar to the harmonic case, the energy behavior for $N \geq 10$ cases is the same for all N-values in short times region while the exponents for higher times are dependent on N. The main consequence of this is that the recurrence of the energy (and the coherence) to the system does not occur anymore for $10 \leq N \leq 20$. The anharmonicity of the Morse potential destroys the recurrences.

The main goal of this work is to show general features which occur in systems coupled to a bath with an increasing number N of constituents. The physical implications of these features for the quantum dynamics of a main system coupled to a finite bath, can be summarized as: decoherence and dissipation decay exponentially for shorter times $t \lesssim t_{disc}$ and are independent of N since the system did not have time to resolve the discreteness of the bath. For longer times, $t \gtrsim t_{disc}$, energy shows a power-law decay for harmonic potential and an exponential decay for Morse potential. In classical conservative systems, power-law decays of the energy [25,26] and the recurrence times statistics are related to sticky motion and memory effects due to a dynamics close to local invariants. This suggests that non-Markovian effects could be expected for the quantum case considered here when power-law decays are observed. In fact we have shown here that recurrences observed for small values of N induce a finite constant non-Markovianity measure, while the exponential and power-law decays of the purity decide how fast the non-Markovianity disappears. In general, for small N the bath *discreteness* tends to induce an energy and coherence *exchange* between system and bath and non-Markovian effects. These properties look somehow related to recent observation which considered flow of quantum correlations from a two-qubit system to its environment [58] and entanglement and non-Markovianity of quantum evolutions [59].

In addition to the above main general results, we would like to conclude with some relevant characteristics observed in the simulations but not mentioned along the text: The energy decay rate increases with increasing the total coupling strength between system and bath, but the time for energy regain is independent of the coupling. The energy regain time depends on the mean bath frequency and on N. For larger N results are totally independent on the numerical frequency generator. For smaller values $1 \leq N \leq 50$, the *values* of exponential and power-law exponents for the energy decay may change for different frequencies generator, but the overall qualitative dynamics is equivalent.

Acknowledgments

MG and MWB acknowledge the financial support of CNPq and FINEP (under the project CTINFRA). They also thank RM Angelo for discussions. Our international cooperation is supported by PROBRAL-DAAD/CAPES.

References

[1] I. Burghardt, M. Nest, G.A. Worth, J. Chem. Phys. 119 (2003) 5364.
[2] L. Ratschbacher, C. Sias, L. Carcagni, J.M. Silver, C. Zipkes, M. Kohl, Phys. Rev. Lett. 110 (2013) 160402.
[3] K.W. Murch, S.J. Weber, C. Macklin, I. Siddiqi, Nature 502 (2013) 211.
[4] M. Sarovar, A. Ishizaki, G.R. Fleming, K.B. Whaley, Nat. Phys. 6 (2010) 462.
[5] G.D. Scholes, Nat. Phys. 6 (2010) 402.
[6] U. Weiss, Quantum Dissipative Systems, World Scientific, Singapore, 1999.
[7] P. Ullersma, Physica 32 (1966) 27.
[8] R. Zwanzig, J. Stat. Phys. 9 (1973) 215.
[9] E. Cortés, B.J. West, K. Lindenberg, J. Chem. Phys. 82 (1985) 2708.
[10] N. Makri, J. Math. Phys. 36 (1995) 2430.
[11] L. Muhlbacher, J. Ankerhold, C. Escher, J. Chem. Phys. 121 (2004) 12696.
[12] J. Casado-Pascual, C. Denk, M. Morillo, R.I. Cukier, Chem. Phys. 268 (2001) 165.
[13] H. Wang, M. Thoss, J. Chem. Phys. 119 (2003) 1289.
[14] K.H. Hughes, C.D. Christ, I. Burghardt, J. Chem. Phys. 131 (2009) 024109.
[15] R. Martinazzo, M. Nest, P. Saalfrank, G.F. Tantardini, J. Chem. Phys. 125 (2006) 194102.
[16] C. Meier, D.J. Tannor, J. Chem. Phys. 111 (1999) 3365.
[17] A. Ishizaki, Y. Tanimura, Chem. Phys. 347 (2000) 185.
[18] W.T. Strunz, T. Yu, Phys. Rev. A 69 (2004) 052115.

[19] W. Koch, F. Grossmann, J.T. Stockburger, J. Ankerhold, Phys. Rev. Lett. 100 (2008) 230402.
[20] C.-M. Goletz, F. Grossmann, J. Chem. Phys. 130 (2009) 244107.
[21] R.P. Feynman, F.L. Vernon, Ann. Phys. 24 (1963) 118.
[22] A.O. Caldeira, A.J. Leggett, Physica A 121 (1983) 587.
[23] L. Diósi, W.T. Strunz, Phys. Lett. A 235 (1997) 569.
[24] W.T. Strunz, L. Diósi, N. Gisin, T. Yu, Phys. Rev. Lett. 83 (1999) 4909.
[25] J. Rosa, M.W. Beims, Phys. Rev. E 78 (2008) 031126.
[26] C. Manchein, J. Rosa, M.W. Beims, Physica D 238 (2009) 1688.
[27] S. Abdulack, W.T. Strunz, M.W. Beims, Phys. Rev. E 89 (2014) 042141.
[28] S. Bay, P. Lambropoulos, K. Molmer, Phys. Rev. Lett. 76 (1996) 161.
[29] J.J. Hope, Phys. Rev. A 55 (1997) R2531.
[30] S. John, T. Quang, Phys. Rev. Lett. 74 (1994) 3419.
[31] N. Vats, S. John, Phys. Rev. A 58 (1998) 4168.
[32] G.M. Moy, J.J. Hope, C.M. Savage, Phys. Rev. A 59 (1999) 667.
[33] Ph. Blanchard, et al. (Eds.), Decoherence: Theoretical, Experimental, Conceptual Problems, in: Lecture Notes in Physics, vol. 538, Springer, Heidelberg, 2000.
[34] W.H. Zurek, Phys. Today (1991) 36. October 1991.
[35] D. Giulini, E. Joos, C. Kiefer, J. Kupsch, I.O. Stamatescu, H.D. Zeh, Decoherence and the Appearance of the Classical World, Springer, Berlin, 1996.
[36] V. Wong, M. Gruebele, Chem. Phys. 284 (2002) 29.
[37] J. Rosa, M.W. Beims, Physica A 342 (2004) 29.
[38] J. Rosa, M.W. Beims, Physica A 386 (2007) 54.
[39] W. Koch, F. Grossmann, J. Stockburger, J. Ankerhold, Chem. Phys. 370 (2010) 34.
[40] Y. Hamdouni, J. Phys. A: Math. Theor. 42 (2009) 315301.
[41] J. Gemmer, M. Michel, Eur. Phys. J. B 53 (2006) 517.
[42] W.T. Strunz, Phys. Lett. A 224 (1996) 25.
[43] T. Yu, L. Diósi, N. Gisin, W.T. Strunz, Phys. Rev. A 60 (1999) 91.
[44] L. Diósi, Quantum Semiclassical Opt. 8 (1996) 309.
[45] I. de Vega, D. Alonso, P. Gaspard, W.T. Strunz, J. Chem. Phys. 122 (2005) 124106.
[46] W.H. Press, S.A. Teukolsky, W.T. Vetterling, B.P. Flannery, Numerical Recipes in Fortran, Cambridge University Press, USA, 1992.
[47] M.A. Marchiori, M.A.M. de Aguiar, Phys. Rev. E 83 (2011) 061112.
[48] Y. Elran, P. Brumer, J. Chem. Phys. 121 (2004) 2673.
[49] A.C.S. Costa, R. Angelo, M.W. Beims, Phys. Rev. A 90 (2014) 012322.
[50] H.-P. Breuer, E.-M. Laine, J. Piilo, Phys. Rev. Lett. 103 (2009) 210401.
[51] A. Rivas, S.F. Huelga, M.B. Plenio, Phys. Rev. Lett. 105 (2010) 050403.
[52] S. Luo, S. Fuo, H. Song, Phys. Rev. A 86 (2012) 044101.
[53] L.D. Lau, E.M. Lifschitz, Quantenmechanik, Akademie - Verlag, Berlin, 1986.
[54] P.-N. Roy, T. Carrington Jr., Chem. Phys. Lett. 257 (1996) 98.
[55] P.M. Morse, Phys. Rev. 34 (1929) 57.
[56] V. Fack, G. Ven Berghe, J. Phys. A: Math. Gen. 20 (1987) 4153.
[57] T. Pang, An Introduction to Computational Physics, second ed., Cambridge University Press, 2010.
[58] G.H. Aguilar, O.J. Farías, A. Valdés-Hernéz, P.H.S. Ribeiro, L. Davidovich, S.P. Walborn, Phys. Rev. A 89 (2014) 022339.
[59] Loss of coherence memory effects in quantum dynamics, J. Phys. B: At. Mol. Opt. Phys. 45 (2012). Special issue, Guest Editors: F. Benatti, R. Floreanini, G. Scholes.